minerals

MDPI

Review

Use of Natural Zeolite Clinoptilolite in the Preparation of Photocatalysts and Its Role in Photocatalytic Activity

Jelena Pavlović [1] and Nevenka Rajić [2,*]

[1] Institute of Soil Science, Teodora Drajzera 7, 11000 Belgrade, Serbia; soils.pavlovic@gmail.com
[2] Faculty of Ecology and Environmental Protection, University "Union, Nikola Tesla", Cara Dušana 62–64, 11158 Belgrade, Serbia
* Correspondence: nrajic@unionnikolatesla.edu.rs

Abstract: The use of natural zeolite clinoptilolite in preparing photocatalysts and its function in photocatalysis are discussed in this review. The importance of advanced oxidation processes (AOPs) and the potential of heterogeneous photocatalysis in removing environmental pollutants are emphasized. The review focuses on the synergistic effects of clinoptilolite with semiconductors (TiO_2, ZnO, CuO, SnO_2, and NiO) to prepare stable and active photocatalysts, highlighting recent advancements in this field. It explores clinoptilolite's structural characteristics, highlighting its microporous nature, adaptable framework, and improved textural properties due to acid and alkali treatments. Particle size, crystal phase, and calcination temperature are three key synthesis parameters that affect photocatalytic activity and are highlighted in the discussion of these parameters and their methods. A discussion is held regarding the processes and mechanisms of photocatalytic degradation of different organic compounds under varying irradiation conditions, including UV, visible, and ambient sunlight. Clinoptilolite is vital in improving supported semiconductor oxides' photocatalytic efficiencies, which aid in pollutant degradation and environmental remediation.

Keywords: natural zeolite; clinoptilolite; photocatalysis; AOPs; semiconductor oxides; photodegradation

Citation: Pavlović, J.; Rajić, N. Use of Natural Zeolite Clinoptilolite in the Preparation of Photocatalysts and Its Role in Photocatalytic Activity. *Minerals* **2024**, *14*, 508. https://doi.org/10.3390/min14050508

Academic Editor: Nikolaos Kantiranis

Received: 26 April 2024
Revised: 9 May 2024
Accepted: 10 May 2024
Published: 13 May 2024

1. Introduction

Natural porous materials like clays and zeolites have drawn a lot of attention in the past decade as safe, cost-effective, and environmentally acceptable components for the making of heterogenous photocatalysts [1–10]. Photocatalysis is one of the most promising advanced oxidation processes (AOPs) [11–16] in which highly reactive oxidants, like the hydroxyl radical (˙OH), which can oxidize pollutants into less hazardous byproducts or completely mineralize them, are generated under mild reaction conditions and with low energy consumption [10,17–20]. A general mechanism of photocatalysis is shown in Figure 1.

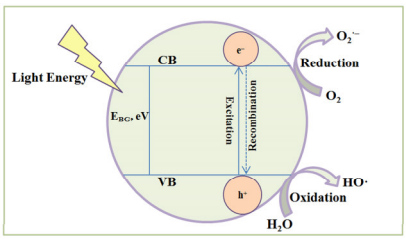

Figure 1. General mechanism of heterogeneous photocatalysis. The photocatalyst is exposed to light that has an energy that is at least equivalent to its band gap energy (EBG), conduction band (CB), and valence band (VB).

In the process, photogenerated holes oxidize H_2O to form $^{\cdot}OH$ radicals, and dissolved O_2 absorbs photogenerated electrons to produce $^{\cdot}O_2$ radicals. Radicals can efficiently oxidize reactive substrates like dye molecules, break down organic pollutants, or oxidize biological species. In contrast to conventional methods for wastewater treatment, heterogenous photocatalysis has demonstrated exceptional potential because the oxidation process requires only water and oxygen as substrates [13,21]. However, it is essential to acknowledge that despite extensive theoretical research on photocatalytic water treatment, numerous obstacles impede the rapid advancement of photocatalysis from theoretical investigation to real-world implementation. First, the yield of oxidative species, such as photogenerated holes and reactive oxygen species (ROS), is severely restricted by the inherent photogenerated electron–hole recombination inside the photocatalyst [22–24]. Second, owing to a short lifetime and non-selectivity, ROS are readily quenched by complex background constituents, such as anions, cations, or natural organic matter [25–27]. Thus, only a minority of photogenerated ROS contributed to the eventual degradation of target pollutants [14,19]. Therefore, the low yield and the poor effectiveness of ROS lead to the unsatisfactory oxidation efficiency of the single photocatalytic oxidation process, which significantly limits its practical application.

This review is focused on applying natural zeolite, clinoptilolite, in photocatalysis. As one of the most abundant natural zeolites, clinoptilolite has been shown not only as a suitable carrier for photocatalytic active species but also as an active participant in the photocatalytic process. Zeolites have drawn interest due to their high surface area, three-dimensional micropore structure, high mechanical and thermal stability, and controllable acidity [28–32]. The porous lattice increases the surface area of photocatalysts and contributes to their recyclability. The review addressed a range of semiconductors, the most commonly studied heterogeneous photocatalysts, whose shortcomings are addressed and whose activity increases in the presence of zeolites.

2. Structural Features of Clinoptilolite

Clinoptilolite is a microporous mineral that is found all across the planet. This makes it an affordable and easily accessible natural material. Its aluminosilicate lattice possesses a unique two-dimensional channel system [33,34]. It consists of three straight channels: A, B, and C. A is the largest and is accessible through a 10-member ring with a free aperture of 5.5 × 3.1 Å; channel B is accessible through a symmetric 8-member ring with a free aperture of 4.1 × 4.1 Å. Access to channels C, A, and B converge through an asymmetric 8-member ring with a 3.4 × 2.8 Å free aperture.

Clinoptilolite has a flexible framework, and compared to other zeolites, it varies more with temperature and composition in terms of cation site occupancies, cell parameters, and free apertures of channels [35]. Figure 2 shows an overview of the clinoptilolite structure projected along the c-axis. Water molecules (W) and extra framework cations (M) are located in cages I and II, at the B and C channel, and A and C channel intersections [36].

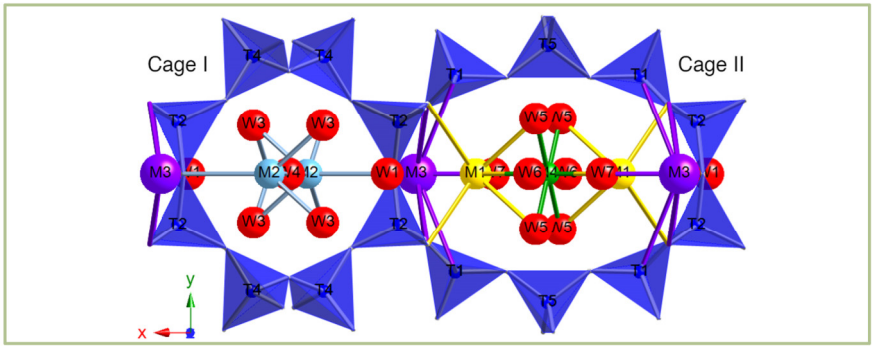

Figure 2. An overview of the clinoptilolite structure projected along the c-axis [36].

Clinoptilolite's aluminosilicate lattice exhibits chemical and thermal stability, allowing for the optimization of its adsorptive and catalytic characteristics. The natural clinoptilolite's textural qualities are enhanced by an acid treatment, which also increases the acidity and Al content [34,37–39]. The widely used alkaline treatment entails hydrolyzing Si in the presence of OH^- to selectively extract it from the structure. This treatment creates mesoporosity and increases accessibility and adsorption capacity. It also enriches the aluminum content, increasing the zeolite's acidic qualities [40–43].

Cations in aqueous media are easily exchanged with those in the channels and cages of clinoptilolite [44]. With its open-framework structure, clinoptilolite has the unique capacity to be used as a nanoreactor due to its microporosity and cations' movability. Thus, calcining transition metal-exchanged clinoptilolite appears as an easy and practical way to prepare different transition metal nanosized oxides on the surface of clinoptilolite [45]. The hydrated cations within the lattice lose water molecules during calcination and move toward the framework's exterior, reacting with oxygen to form oxides. Chanel aperture influences particle size, and channel system geometry inhibits their agglomeration.

A preparing transition metal sulfide and halide particles on the clinoptilolite surface follows a similar principle [46–48]. Insoluble transition metal sulfide (halide) is formed on the surface of transition metal-exchanged clinoptilolite upon treatment with a sulfide (halide) water solution. The reaction appears to be driven primarily by the precipitation of slightly soluble products.

Different methods are used to prepare photocatalysts based on clinoptilolite, suggesting that the synthesis method considerably influences the catalyst composition and photocatalytic performance. Metal oxides on the clinoptilolite can be introduced via precipitation, ion exchange, impregnation, hydrothermal, sol-gel, or solid-state dispersion [3,49–52]. Synthesis parameters, including metal concentration, reaction temperature and time, and calcination temperature, affect the photocatalytic activity by creating active sites on the clinoptilolite support. For example, calcination temperature is responsible for developing both crystallinity and textural properties, which directly affect the activity of photocatalysts. Since each synthesis method has advantages and limitations, careful optimization of the synthesis parameters is necessary to create the photocatalytic active sites.

2.1. Photocatalytic Activity of Semiconductor Oxides

2.1.1. TiO_2

Because it is an inexpensive and photostable substance, titanium dioxide has been the most investigated semiconductor in photocatalysis. Due to its band gap (EBG) of 3.2 eV, it absorbs the ultraviolet spectrum. A valence band (VB) electron (e−) in TiO_2 absorbs photon energy and is excited to the conduction band (CB) when exposed to light with a wavelength of <387 nm [53–56]. In the course of this, a hole (h+) is made in the VB. This process results in the generation of an e/h pair and the formation of the photo-excitation state. A hole in an acceptor that oxidizes donor molecules is reduced by this excited electron. Since a photocatalyst can offer an environment for oxidation and reduction simultaneously, it is vital for the process. The extent of recombination of the photoexcited electron–hole during the photocatalytic process determines the photocatalytic reaction's efficiency. Its high rate of photogenerated electron–hole pair recombination, particle aggregation, and ineffective recovery hinder the photocatalytic activity and efficient exploitation of TiO_2. Immobilizing TiO_2 particles on high porous supports provided a suitable method to address the previously mentioned drawbacks. It has been reported that zeolite porous structure, morphology, and surface charges considerably promote the recovery efficiency of TiO_2 particles following photocatalytic reaction and prolong the separation of the charged species [57]. TiO_2 supported on clinoptilolite matrix, which was previously modified by alkaline treatment, increases the photocatalytic activity of TiO_2 up to 57%. It is explained by the fact that the photogenerated electrons delay the

recombination of electrons and holes by hopping from one acid site to another inside the zeolite lattice as they move from TiO_2 to the zeolite matrix. Without a zeolite matrix, photogenerated electrons will quickly transfer to the VB of TiO_2 owing to the instability of excited states. The alkaline zeolite treatment increases the relative content of Al^{3+} because some Si^{4+} is leached and enhances the effect of the delay of electron–hole recombination.

Salicylate acid (SA) breakdown in an aqueous solution can be effectively catalyzed by TiO_2-supported clinoptilolite produced by metal–organic chemical vapor deposition. Results showed that compared to commercial P25 Degussa, the prepared catalyst ultimately needed less irradiation time to degrade SA. The catalyst has exceptional stability as it may be recycled up to four times without experiencing any decrease in activity [58]. The reason behind this was attributed to the clinoptilolite surface, which can effortlessly absorb ·HO radicals on TiO_2 surfaces. It is implied that the formation of the ·HO presents a chance for the SA molecules, which have already been adsorbed on the photo-inert clinoptilolite, to be broken down, increasing the photodegradation efficiency. However, when Ti–O–Si hetero-linkages are present on the catalyst, it is hypothesized that positive ion defects occur. The interaction between the oxygen on the zeolite surface and the high positive ion, Ti(IV), may result in an electron trapping effect at the interface between TiO_2 and clinoptilolite. The catalyst exhibits enhanced photosensitivity through a modest delay in recombining the photogenerated electron–hole pair. The preparation process also significantly increases the clinoptilolite matrix's specific surface area (more than ten-fold). A Ti(IV)–salicylate surface complex was proposed to be formed, with a high mesopore count facilitating improved interaction between SA molecules and Ti sites. SA removal effectiveness is increased by the combination of photodegradation and adsorption.

To modify the electronic band structure of TiO_2, different methods have been employed to widen the band gap to the visible light region of the solar spectrum ($\lambda > 400$ nm), enhance photocatalytic activity in the solar range (the band gap of TiO_2 should be less than 3 eV), and prevent electron/hole pair recombination. TiO_2's optical capabilities are affected by the transition metal doping-induced insertion of intermediate bands into its narrower forbidden gap. Because of this, the wavelength at which visible light is absorbed is shifted, leading to an increase in light absorption [59]. TiO_2 catalysts doped with Cu, Fe, and Fe/Cu immobilized onto clinoptilolite have recently been prepared using a unique electrochemical-thermal technique disclosed. Cu(II) doping efficiently narrows TiO_2's broadband gap, but Fe^{3+} doping creates oxygen vacancies in the crystal lattice and on the surface, promoting the attachment of water molecules and the development of hydroxyl groups. Theoretically, this might enhance the catalyst's activity toward pollutant degradation under UV–VIS irradiation by acting as electron or hole scavengers and improving the separation of free charges [59]. Combining the photocatalytic activity of TiO_2 with the adsorption properties of zeolite, TiO_2 supported on clinoptilolite creates a synergistic effect that increases photocatalytic efficiency.

The size of the clinoptilolite particles that are employed to immobilize TiO_2 has an impact on its photocatalytic activity. When clinoptilolite particles are added to support TiO_2, Zabihi-Mobarakeh and Nezamza-deh-Ejhieh [60] state that this increases the photocatalytic effectiveness in photodegradation of an aqueous solution containing a combination of aniline and dinitroaniline. The efficiency improvement of clinoptilolite nanoparticles is more significant than micronized particles. According to the results, photogenerated electrons can be dispersed across the zeolitic support's network structure, which inhibits the recombination of electron–hole pairs and raises the supported TiO_2's photodegradation efficiency.

Nanosized TiO_2-supported clinoptilolite [61] created a new paper composite with excellent photocatalytic activity. Sol-gel-generated TiO_2 colloids were used to develop photocatalytic material coupled with clinoptilolite. Using as-prepared anatase TiO_2 on zeolite particles, the photocatalytic publication showed that TiO_2-zeolite particles were

distributed throughout a microvoid-filled, dense network of fibers. When exposed to UV light, the photocatalytic composite paper broke down the gaseous toluene very effectively, outperforming commercial photocatalytic non-woven paper from Ahlstrom or photocatalytic paper manufactured with Degussa P25 TiO_2. The organic contaminants were eliminated through the combined action of three processes: (1) confinement of the contaminants in microvoids between fiber networks, (2) further adsorption of the contaminants on clinoptilolite, and (3) subsequent photodecomposition of the adsorbate by TiO_2 nanoparticles.

The synthesis of anatase TiO_2-containing clinoptilolite was carried out using the sol-gel method, and the resultant photocatalyst showed activity in the UV-induced degradation of monoethanolamine, which is employed in the gas and oil refining process [62]. Within 100 min, over 90% of the monoethanolamine was broken down, demonstrating the anatase-clinoptilolite catalyst's superiority over pure anatase (20%). This was explained by the exceptional capacity of clinoptilolite to collect organic materials close to TiO_2 particles and the ease with which hydroxyl radicals from TiO_2 surfaces can adhere to the surface of clinoptilolite. Furthermore, positive ion defects could result from newly formed Ti–O–Al and Ti–O–Si bonds. Due to the coupling of a high positive ion, Ti^{4+}, with the surface O atoms in the clinoptilolite lattice, they can function as the electron trapper at the interface of the clinoptilolite and TiO_2.

Under UV light, the antibiotic sulfadiazine is actively degraded by the photocatalyst based on TiO_2 particles with a particle size of roughly 50 nm and clinoptilolite made using the sol-gel process [63]. Reactive oxygen species that are highly active oxidative species, such as OH, $\cdot O_2^-$, HO_2, and $^1O_2$, have been observed to react with adsorbed sulfadiazine molecules on the surface of the photocatalyst. Additionally, the sol-gel method successfully synthesizes TiO_2 nanoparticles dispersed over dealuminated clinoptilolite to degrade organic colors [64]. The decrease of partial aggregation of TiO_2 nanoparticles, an enhanced absorption edge for more significant photon generation, and the efficient separation of photogenerated charge carriers by clinoptilolite-supported photocatalyst were revealed to be significant factors influencing its activity. Following a 180 min UV light exposure, the dye degradation rates for Methylene blue and Methyl orange were 83% and 94%, respectively.

According to Ullah, the crystal phase and particle size of TiO_2 supported onto clinoptilolite significantly impact the photocatalytic degradation of crystal violet under UV light [51]. The anatase phase has the highest activity because its crystals have the proper size, shape, and distribution. Ullah et al. [52] investigated the relationships between synthesis techniques and the physicochemical properties of the resultant TiO_2-supported clinoptilolite by utilizing a range of techniques, such as sol-gel, hydrothermal, and in situ hydrothermal procedures. Unlike the sol-gel and hydrothermal methods, the in situ hydrothermal approach produces well-dispersed TiO_2 particles and minimal particle aggregation while maintaining the clinoptilolite crystal structure intact. These two techniques produce aggregated TiO_2 and cause the zeolite lattice to partially deform.

Three times more effective than ZnO-supported clinoptilolite, TiO_2-supported clinoptilolite showed outstanding photocatalytic activity in degrading dangerous Rhodamine B dye under UV irradiation. With a 93% rate, TiO_2-supported clinoptilolite has exceptional reclining resilience. Superoxide ($\cdot O_2-$) and hydroxyl radicals ($^{\cdot}OH$) were the most active species in the photodegradation of both materials, with photoexcited holes (h+) having a tiny impact [6]. Better TiO_2 particle dispersion onto the clinoptilolite surface explains the higher photocatalytic activity.

On the surface of acid-treated clinoptilolite, anatase TiO_2 was hydrothermally prepared with a size of roughly 20 nm and high dispersity [50]. The synergistic impact of TiO_2 and the clinoptilolite lattice is responsible for the rapid breakdown of sodium isopropyl xanthate under UV light irradiation (approximately 90% within 30 min with a dosage of 1.0 g dm^{-3}). Only a tiny amount of ·OH and e− are formed during degradation, as evidenced by the free radical experiment, which showed a modest drop in degradation

efficiency upon adding $AgNO_3$ and isopropanol. On the other hand, the presence of 1,4-benzoquinone and edentate disodium causes a significant drop in the degradation efficiency, suggesting that O_2− and h+ are the predominant reactive species during the process. Figure 3 depicts a potential photocatalytic system.

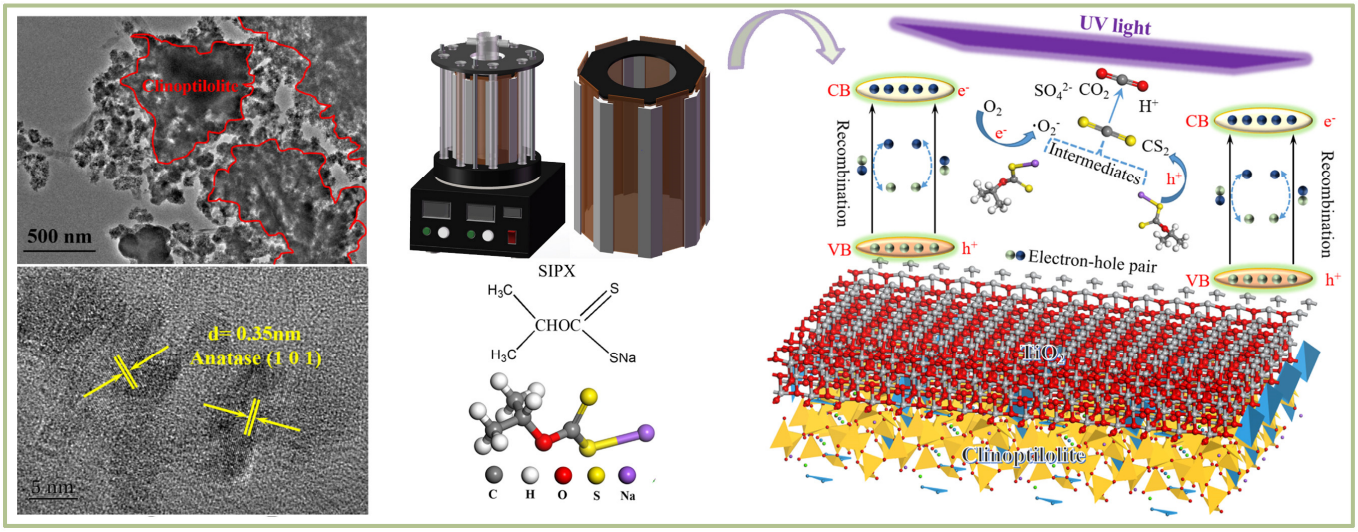

Figure 3. Photocatalytic mechanism of sodium isopropyl xanthate (SIPX) degradation on the surface of TiO_2-clinoptilolite under UV light [50].

The aqueous terephthalic acid solution was degraded under UV light by photocatalytic activity, and the spherical rutile TiO_2 clusters onto clinoptilolite were created by acid hydrolysis of a $TiCl_4$ solution without a calcination step [65]. Despite less active TiO_2, the photocatalyst with a rutile/zeolite weight ratio of 0.5 was the most photoactive of the catalysts made with various rutile to zeolite weight ratios. In addition, the catalysts have greater catalytic activity than anatase and Degussa P25 sold in stores. The Langmuir–Hinshelwood model suggested that adsorption had little role in the degradation process.

Under visible light irradiation, a novel BiOCl-TiO_2-clinoptilolite photocatalyst produced by precipitation and calcination exhibits outstanding photoactivity in the degradation of Rhodamine B [66]. Compared to pure TiO_2, BiOCl, and TiO_2-clinoptilolite composite, the pseudo-first-order kinetic constant is 48, 11, and 30 times greater, respectively. Better adsorption capacity and developing the n–p heterojunction between BiOCl and TiO_2 are responsible for the increased photocatalytic activity. This creates a quick adsorption–desorption system and facilitates the effective separation of the photogenerated electron–hole pairs. The band gap width of Bi-OCl-TiO_2-clinoptilolite (2.88 eV) is less than that of pure BiOCl (3.39 eV) and pure TiO_2 (3.14 eV) because of the heterojunction effect. The active radical tests show that hydroxyl radicals and holes are responsible for Rhodamine B's breakdown.

When exposed to visible light, the hierarchical MoS_2-TiO_2-clinoptilolite, synthesized by a mild hydrothermal method, exhibited improved photodegradation activity towards common Na-based xanthates [67]. When the molecular weight of the xanthate rose, the degradation efficiency grew progressively, and within three hours, it reached over 90% for sodium isopropyl xanthate. The results of the radical scavenger tests indicate that superoxide radical anions (O_2^-) are the main active species and that the ·OH species are secondary to them in the photodegradation process. In addition to demonstrating photoactivity in the breakdown of xanthates under visible light irradiation, a unique ternary Ag-TiO_2-clinoptilolite nanocomposite was also created using a two-step synthesis technique that combined the hydrothermal and in situ reduction procedure [68]. Ag

nanoparticles on TiO_2-clinoptilolite's surface aid in separating photoinduced carriers and improving the material's capacity to absorb visible light.

A recent report reported that carbon-doped TiO_2 supported onto clinoptilolite effectively catalyzed the degradation of organophosphorus pesticides (glyphosate and diazinon) under visible light. This suggests that non-metal dopants could also be a suitable way to increase the photocatalytic activity of TiO_2 [69]. Sodium carboxymethyl cellulose was used as a C source in the sol-gel synthesis of a photocatalyst. An average of 43 nm in diameter spherical TiO_2 particles were produced. The synthesized photocatalyst absorption edge was raised in accordance with the UV-Vis diffuse reflectance spectrum. Furthermore, 3.2, 2.9, and 2.76 eV were determined to represent the band gap energies of pure TiO_2, C-doped TiO_2, and C-doped TiO_2-clinoptilolite, respectively. Under ideal circumstances, which included an initial pesticide concentration of 30 mg dm^{-3}, a pH of 3 for glyphosate and 6 for diazinon, and a catalyst dosage of 0.3 g dm^{-3}, the degradation efficiencies of 84% and 89.67%, respectively, were achieved for the two chemicals. Including scavengers such as tert-butanol, 1,4-benzoquinone, and ammonium oxalate reduced the photocatalytic breakdown of both insecticides, but to differing degrees. Although activity declines in the following order, all three radicals are essential in the breakdown of the pesticides; glyphosate has $h^+ > {}^{\cdot}O_2^- > {}^{\cdot}OH$ and diazinon has ${}^{\cdot}OH > h^+ > {}^{\cdot}O_2^-$ [69].

2.1.2. ZnO

ZnO is a typical n-type semiconductor used as a UV photocatalyst because of its high chemical stability, low cost, wide bandgap (about 3.2 eV), and chemical inertness. ZnO exhibits significant potential in photocatalysis, particularly in the degradation of organic pollutants, due to its tunable size, high chemical stability, low toxicity, and ease of preparation [70–74]. Wide band gap and rapid electron–hole pair recombination rate are two of ZnO's disadvantages as a photocatalyst, which lower the photodegradation efficiency of the bare ZnO photocatalyst.

The photoactivity is enhanced by the high surface area and nanostructured ZnO particles; however, the dispersion and recovery of nanosized ZnO material at the end of the process was challenging. ZnO was modified with an inert or active material to improve its adsorption capabilities and catalyst efficiency, which solved the problem and permitted an easier recovery by filtration or deposition. One of the effective methods for creating hybrid catalysts that can effectively separate from the reaction system and disperse neatly is impregnation. Nano ZnO-impregnated clinoptilolite effectively decomposes benzophenone and caffeine exposed to UV light. Zeolite enhances adsorption properties, catalyst efficiency, and recovery [75].

The photocatalytic degradation of 4-nitrophenol by ZnO was increased by supporting it onto the nano clinoptilolite. The photocatalyst was prepared by ion exchanging the nano clinoptilolite followed by calcination [76]. It was concluded that the role of the clinoptilolite support is essential in the photodegradation process since pure ZnO does not show a significant photodegradation efficiency.

Nano ZnO supported onto clinoptilolite is photocatalytically active in the photodegradation of aromatic amine (2,4-dichloroaniline) under Hg lamp irradiation [77]. The photodegradation rate drastically increases by the oxide supporting. This was ascribed to the clinoptilolites' permanent internal electrical field, which interacts with the photoinduced e−/h+ pairs to separate them and its ability to prevent aggregation. The best photodegradation rate was obtained in moderate acidic media (pH = 5–6) in which 2,4-dichloroaniline was present in the neutral form, and the photocatalyst surface had a net positive charge. The content of ZnO on clinoptilolite does not influence the degradation rate.

Compared to unsupported ZnO, the supported ZnO on the surface of micro- and nano-sized clinoptilolite exhibited significantly higher photocatalytic efficiency toward phenylhydrazine. Clinoptilolite enhanced photocatalytic activity by preventing ZnO

particle aggregation. The larger surface area of the nano-sized zeolite enhanced the photodegradation efficiency of ZnO particles to a greater extent than the micro-sized zeolite. This confirms that the right milling conditions can produce clinoptilolite powders with particle sizes less than 100 nm and desired crystallinity, significantly increasing the photodegradation process's efficiency [78]. A similar effect is reported for the photo decolorization of bromothymol blue under Hg lamp irradiation [79].

Compared to photocatalysts prepared by conventional precipitation, ZnO prepared by the sono-precipitation method showed a better photocatalytic performance for the degradation of furosemide under UV irradiation [49]. Discreet, non-agglomerated ZnO nanoparticles with uniform morphology and nanoparticles of 20.5 nm size were obtained. Moreover, the specific surface area increased twice compared to conventional precipitated photocatalysts. Based on the results of the scavenging tests, the highest reduction in degradation efficiency occurred in the presence of ammonium oxalate monohydrate and tert-butanol, indicating h+ and ·OH as the main responsible reactive species in the degradation of furosemide. It is suggested that electrons of the ZnO conduction band are transferred to the clinoptilolite nanorods, which serve as electron sinks and, by inhibiting the e−/h+ recombination, contribute to the degradation, demonstrating the important role of clinoptilolite in the degradation process.

The degradation of the organic dyes Methylene blue and Rhodamine B has recently been investigated and compared with the photocatalytic activity of ZnO supported on clinoptilolite and zeolite A [80]. The ZnO surface area in the clinoptilolite-based composite is reported to have decreased somewhat. Nevertheless, the ZnO-zeolite A showed a noticeable decline. The composites have band gaps that range from 3.18 to 3.21 eV. The conclusion that using semiconductor oxides supported on zeolites is a practical and effective process in reducing contaminants present in wastewater is reached when the photocatalytic performance increases by about 60%.

ZnO-supported clinoptilolite obtained by wet impregnation showed excellent efficiency (96%) in the photodegradation of hydroxychloroquine. Ecotoxicological tests suggested that the toxicity of the synthetic effluent after the advanced oxidative treatment had been reduced (used frequently during the COVID pandemic) [81].

The photocatalytic reduction of Cr(VI) over Ag-doped ZnO-containing clinoptilolite has been reported by Wahyuni et al. [82]. The doping Ag presumably reduces the band gap energy of ZnO to 2.80 eV, which significantly increases the photocatalyst's activity. Reaction time, photocatalyst mass, and solution pH are the main determinants of photocatalytic performance. The photocatalytic efficiency of ZnO and FeO supported on clinoptilolite is significantly increased by their hybridization and immobilization in the clinoptilolite lattice. It has been reported that electron–hole recombination was reduced considerably, leading to an increase in photocatalytic efficiency due to charge separation that arises from excited photoelectrons migrating from the FeO (2.1 eV) conduction band into the ZnO (3.2 eV) conduction band. The ZnO/FeO ratio highly influences the degradation efficiency; the composite with 4.1% ZnO and 4.3% FeO exhibited the best results. Moreover, it is noticed that the production of reactive radicals is possible by adjusting pH. At more acidic and basic pHs, less reactive OCl and HO_2 form, reducing the degradation, whereas more potent OH radicals form at pH ~ 8 [83].

2.1.3. CuO

With an energy band gap of 1.2 to 1.5 eV, copper oxide, a crucial p-type semiconductor, absorbs UV and visible light. Many organic compounds undergo oxidative change due to reactions involving the Cu^{+}/Cu^{2+} pair. Cu may undergo redox reactions with both inorganic and organic substances because of its unique electronic characteristics, which include spin-restricted O_2 [84,85]. Soori and Nezamzadeh-Ejhieh prepared CuO onto clinoptilolite nanoparticles for photodegradation of a 2,6-dimethyl phenol aqueous solution [86]. CuO's photocatalytic activity was enhanced when clinoptilolite nanoparticles were used with CuO. Supporting led to a blue change in CuO's

band gap energy, indicating that CuO nanoparticles had formed within or on the zeolite surface [86]. Direct photolysis had just a tiny part in the dimethyl-phenol removal process. In the presence of Hg Lamp illumination, the micronized and nanosized clinoptilolite showed relative participation in photodegradation, with the latter playing a preferable function. Certain Al–O, and Si–O bonds in the clinoptilolite lattice are hypothesized to have semiconducting properties and to produce particular reactive species in response to light. Additionally, CuO species were scattered throughout the clinoptilolite's surface, which can result in increased photodegradation efficiency and e/h separation. CuO species photoexcited electrons can interact with the internal electric field of zeolites and migrate across the aluminosilicate framework thanks to this property. Consequently, the zeolite-supported CuO may undergo reduced e/h recombination [87].

The photodegradation of combining the anionic dye Bromphenol blue and the cationic dye Methylene blue has been studied using CuO immobilized on clinoptilolite nanoparticles obtained by ion exchange reaction and calcination [88]. The photocatalyst containing 4.9 wt. % CuO had the highest effectiveness among the prepared photocatalysts with varying CuO contents (ranging from 3.3 to 6.7 wt.%), indicating an ideal semiconductor oxide content on clinoptilolite. The agglomeration of CuO particles at greater concentrations of CuO substantially inhibited photon penetration. As a result, fewer OH radicals were generated since fewer CuO particles were accessible to receive photons due to a drop in the effective surface area. Furthermore, higher efficiency was noted for Methylene blue because, in an assault by hydroxyl radicals, the positive charge on the N and S atoms—good leaving groups—caused the cleavage of C–N and C–S bonds. There has also been a report on the significance of CuO content in clinoptilolite for the photocatalytic degradation of 2,4-dichloroaniline [89]. With 3.9 wt. % CuO and 300 min at pH = 3, the photocatalyst reached a degradation rate of 90%.

It has been reported that p-aminophenol, extensively used in the textile industry, degrades under sunlight by CuO-supported clinoptilolite prepared through wet impregnation [90]. Because electron–hole pair recombination is prevented when clinoptilolite is used as a support, the degradation rate increases significantly. Similar outcomes for the UV irradiation-induced photodegradation of benzene-1,2-diamine have been documented [91].

Utilizing a Hg Lamp to irradiate mefenamic acid, the support and hybridization of ZnO and CuO semiconductors on clinoptilolite significantly increased photoreactivity [92]. The enhanced photocatalytic activity is attributed to the linked system's ability to transport photogenerated electrons from the CuO conduction band to the ZnO valence band. This transfer significantly inhibited e/h recombination. The rate of deterioration rose with an increase in ZnO and CuO content, particularly for CuO content. Nonetheless, the system's production rate was limited by the excitation of CuO, and the formation of additional e/h pairs resulted in a rapid transfer of generated photoelectrons from CuO-VB to ZnO-VB.

Recently, a hydrothermal method was successfully used to create a new ternary heterogeneous $BiVO_4$-CuO-supported clinoptilolite [93]. The parent clinoptilolite underwent modification before synthesis via the dealumination–desilication process. When the new catalyst was exposed to light, dibenzothiophene broke down. Since $BiVO_4$ is a negative-type semiconductor and CuO is a positive-type semiconductor, combining the two produces a p–n heterojunction. Figure 4 shows the suggested photocatalytic oxidative desulfurization pathway. The results showed that the ternary composite, created by adding zeolite to the $BiVO_4$–CuO heterojunction, significantly reduced the band gap and increased the composite's overall surface area. Under visible light, 94.7% of the dibenzothiophene was broken down in 30 min, indicating an accelerated sulfur degradation over pure $BiVO_4$.

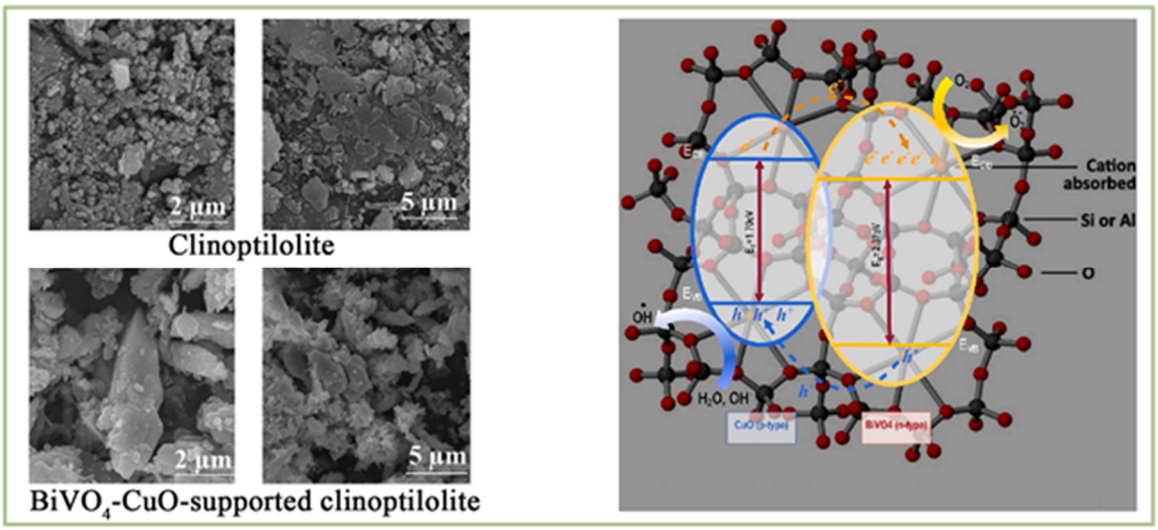

Figure 4. The proposed mechanism for the photodegradation of dibenzothiophene under visible light over p–n heterojunction semiconductors is that the reactive OH^- and O_2^- species are prominent and superior in the degradation process [93].

2.1.4. SnO_2

SnO_2 is an n-type, chemically stable semiconductor with a band gap of 2.9–3.6 eV and excellent electrical and optical properties that make it suitable for the fabrication of photocatalysts. Unlike TiO_2, SnO_2 does not negatively impact health because of its low body absorption, making it a more acceptable photocatalyst than TiO_2. However, due to the simultaneous formation of SnO_2 and SnO during synthesis, SnO_2 has primarily been used as a component of composite photocatalysts, such as SnO_2/ZnO or SnO_2/TiO_2 [94,95].

Photocatalitically active SnO_2 supported onto clinoptilolite was prepared by treatment of clinoptilolite with an alkaline solution of $SnCl_2$ followed by calcination [96]. A photocatalyst with an average size of SnO_2 agglomerates of 19 nm onto the clinoptilolite surface was obtained. The photocatalytic activity is ascribed to the synergistic effect of the SnO_2 particles with cassiterite crystal structure and clinoptilolite lattice. Increasing SnO_2 content over optimal decreased the degradation rate of the dye, which is attributed to the SnO_2 aggregation and decrease in the effective surface area.

Under UV light, the mixture of 4-methyl benzoic acid and 2-chloro-5-nitro benzoic acid was efficiently degraded by the SnO_2-ZnO-clinoptilolite prepared by wet impregnation and calcination [97]. It is suggested that the photogenerated electrons readily migrate to the CB of SnO_2, which significantly prevents e-/h+ recombination and increases photocatalytic activity. This is because ZnO has a more negative CB potential than SnO_2. The content of both SnO_2 and ZnO affects the degradation yield of both pollutants, with ZnO content increasing the most.

In the photocatalytic degradation of metronidazole exposed to moderate pressure Hg lamp radiation, the benefits of coupling SnO_2 and ZnO, and their support onto clinoptilolite have also been reported [98]. Because ZnO and SnO_2 form distinct crystallite phases, the mole ratio of SnO_2/ZnO, calcination temperature, and time all affect the photocatalytic activity. According to the reported data, this catalyst exhibits the highest charge transfer efficiency compared to other catalysts and shows higher photodegradation activity due to a lower e/h recombination. Increased photocatalytic activity in the degradation of a metronidazole aqueous solution was achieved by coupling and supporting NiO and SnO_2 onto clinoptilolite nanoparticles. Nanoparticles were obtained by calcinating Ni(II)-Sn(IV)-exchanged clinoptilolite. A high crystalline NiO–SnO_2 system has higher photocatalytic activity than an amorphous one. Due to its critical role in preventing e/h recombination, the mole ratio of SnO_2/NiO also altered the photocatalytic activity. Since increasing the amount of SnO_2 increased the system's

activity, SnO_2 acted as an electron sink in the SnO_2–NiO system, confirming that recombination of e/h is the rate-limiting step for the photocatalytic activity [99].

SnO_2 and CuO were prepared for the first time and anchored on clinoptilolite using a green technique free of any potentially hazardous surfactant or reducing agent to boost photocatalytic efficiency. Rosmarinus Officinalis worked well as a reducing, stabilizing, and capping agent for biosynthesis. A total of 90% of cefxime was degraded by the biosynthesized SnO_2/CuO-clinoptilolite under natural sunlight. Cefixime was eliminated by the composite 4.15 and 1.81 times quicker than by intact bare SnO_2 and CuO, respectively. All active species were involved in the breakdown of cefxime, but positively charged holes (h+) played a more important role than others [100].

2.1.5. NiO

NiO, a p-type semiconductor with a broad energy band gap of about 3.4–4.0 eV, is suitable for photocatalytic reactions [101–103]. However, its photocatalytic performance is restricted because of its limitations associated with poor adsorption performance and difficulties in the migration and separation of electron–hole pairs. By coupling NiO with other semiconductors, especially their support on porous carriers such as clinoptilolite, photocatalytic activity can be significantly enhanced.

The degradation of antibiotics like cephalexin, cefixime, cefuroxime, and cotrimaxazole under Hg Lamp irradiation is demonstrated by NiO supported onto clinoptilolite nanoparticles prepared by ion exchange followed by calcination [104–107]. The amount of NiO strongly influences the antibiotic degradation rate supported by clinoptilolite, a photocatalyst containing 13.3 wt.% NiO exhibits the best activity. Clinoptilolite's adsorption capabilities increase the likelihood that hydroxyl radicals will target the adsorbed antibiotic molecules, accelerating their breakdown. The chemical oxygen demand tests verified the antibiotics' mineralization. The HPLC chromatograms verified the reported data, which indicate that most of the molecules were reduced to smaller species (primarily inorganic compounds) during irradiation. A partial decrease in activity was reported, but it remained at roughly 70% of its initial activity after three cycles. The attack of hydroxyl radicals caused the cleavage of the C–N bond, which in turn caused the transformation of the organic nitrogen to NO_3^-, NO_2^-, and NH_4^+ ions, whereas CO_2 and H_2O yielded from the C, H, and O. Regeneration of photocatalysts at about 700 °C caused the removal of the adsorbed intermediate products and provided their use in additional reaction cycles. Aromatic amine 2,4-dichloroaniline, a precursor for producing some herbicides, can also be degraded under Hg irradiation using NiO supported onto clinoptilolite [108]. It has been reported that the Langmuir–Hinshelwood model well described the photodegradation, suggesting a faster rate at the optimal conditions, including the catalyst dose: 0.5 g dm^{-3}, an initial conc. of 5 mg dm^{-3}, and the initial pH = 3.

2.2. Other Semiconductors

Because of their availability, versatility, and low toxicity, copper sulfides are recognized as significant p-type semiconductors. CuS is a semiconductor with a band gap between 1.2 and 2.5 eV [109–111]. The Cu 4s state predominates at the bottom of the CB, while well-hybridized states of Cu 3d and S 3p states make up the top of the VB. An examination of the symmetry of these states led to the conclusion that the band gap of CuS is a direct-allowed transition type. Additionally, it was revealed that the significant hybridization of the Cu 3d and S 3p states was the reason for the VB's relatively large dispersion. This dispersed VB causes the appearance of p-type electrical conduction in this material. However, compared to conventional n-type conducting materials, the dispersion of the CB is relatively small, most likely due to the CuS-layered structure. CuS has a wide band gap and high exciton stability due to the CD's small dispersion.

The photoefficiency of the CuS supported by clinoptilolite was studied regarding the decolorization extent of an aqueous solution containing Methyl orange and Bromocresol green [46]. The photocatalyst showed high efficiency in decolorization. A major rate-

limiting factor controlling the photocatalytic efficiency upon the band gap excitation of CuS is the high degree of recombination between photogenerated electrons and holes in the CuS-incorporated clinoptilolite.

NiS is a p-type semiconductor with a narrow band gap of about 0.5 eV, responds to both visible and infrared light, and has two common crystal structures, hexagonal and rhombohedral [112–114]. Owing to its unique properties like a metal-insulator, paramagnetic–antiferromagnetic phase change, low-temperature processable, and high electrical conductivity, NiS finds use as electrodes in lithium-ion batteries, solar cells, supercapacitors, and photocatalytic hydrogen generation [115,116]. NiS can produce hydroxyl radicals during the photocatalytic processes, making it suitable for the degradation of different environmental pollutants. Prospective photocatalysts can be obtained by supporting NiS on minerals such as zeolites.

Furfural, a cyclic aromatic aldehyde, is photodegraded by UV light using NiS supported onto clinoptilolite [117]. As shown by photocatalytic tests, NiS particles loaded onto clinoptilolite represent active centers for furfural degradation. With optimal reaction conditions (pH = 5, 330 mg dm^{-3} of catalyst, and 6 mM of furfural), the photocatalyst degrades about 50% of furfural in 4 h. Photodegradation efficiency is increased when hydrogen peroxide and potassium bromate are added.

PbS is a semiconductor with a band gap of 0.4 eV. It is used in solar batteries, photonic materials, sensors, and hybrid solar cells because of its optical and electrical characteristics [118–120]. An efficient photocatalyst for mineralizing cefotaxime was produced by supporting PbS onto clinoptilolite nanoparticles [121]. It was possible to achieve a cubic PbS phase with crystallite sizes of 17 nm by an ion exchange reaction and sulfidation. Cefotaxime degraded at 82% when PbS-supported clinoptilolite was used but only 38% and 46% when pure clinoptilolite and PbS were used. The photodegradation of the antibiotic ciprofloxacin has demonstrated the significance of the synergistic effect between PbS and clinoptilolite nanoparticles [48]. The catalyst can be reused four times with optimal reaction parameters while retaining roughly 76% of its original activity.

Iron sulfides are also considered competitive materials for photocatalytic processes due to their low cost, natural abundance, negligible toxicity, and optical and electric properties [122]. FeS (band gap energy of 1.95 eV) and Fe_2S_3 (band gap energy of 1.95 eV) semiconductors, coupled and supported onto clinoptilolite nanoparticles by the sulfiding of Fe(II)- and Fe(III)-exchanged clinoptilolite, can be obtained for photodegradation of ciprofloxacin irradiated by W lamp [123]. The diffuse reflectance spectroscopy results suggest that the supported monocomponent FeS or Fe_2S_3 semiconductors show higher band gap energies than the unsupported ones because of the formation of semiconductor nanoparticles on the clinoptilolite. Furthermore, the supported bicomponent FeS–Fe_2S_3 system shows lower band gap energies than the mono-component since the bicomponent system creates mixing energy levels, which results in improved charge separation. Consequently, coupled FeS-Fe_2S_3 exhibits substantially more activity than the monocomponent, indicating that the coupled system's charge transfer is superior. Moreover, the molar ratio of the FeS/Fe_2S_3 plays a crucial role in determining the photocatalytic activity.

Under Hg lamp irradiation, supported PbS–CdS on clinoptilolite nanoparticles demonstrates excellent photocatalytic activity for deleting tetracycline and cephalexin antibiotics in an aqueous solution. Since adding isopropanol, an efficient OH scavenger, significantly reduced the degradation efficiency, OH is responsible for the degradation of pollutants [124]. To solve difficulties in the separation and recovery of photocatalyst, CdS–PbS immobilized onto magnetized clinoptilolite was prepared, and its photocatalytic performance was tested in the degradation of antibiotic cefotaxime under the illumination of a medium-pressure Hg lamp [125]. The best degradation rate was obtained for the photocatalyst containing 6.2% CdS and 5.1% PbS. The scavenging tests indicated a decreased trend in the overall photodegradation efficiency: isopropyl alcohol > carbonate > hydrogen peroxide. The saturation magnetization value indicates the high paramagnetic

properties of CdS/PbS-clinoptilolite, suggesting an easy separation by an external magnetic field. The reported results confirm the critical role of the photoinduced holes in the photodegradation mechanism and propose the direct Z-scheme mechanism (Figure 5) as a favorable mechanism to describe the degradation of cefotaxime.

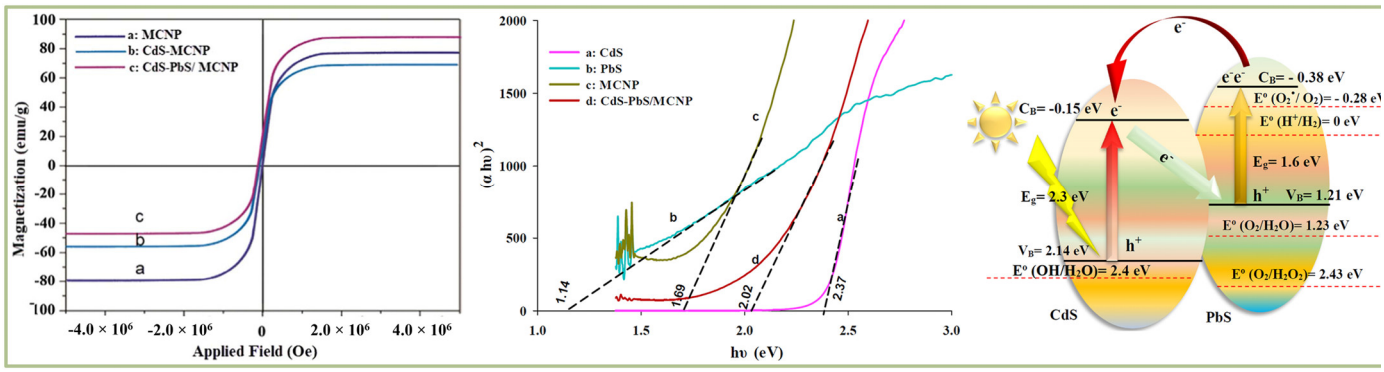

(**a**) (**b**) (**c**)

Figure 5. (**a**) Vibrating sample magnetometer curves; (**b**) typical Tauc plots; and (**c**) the charge carrier separation in the clinoptilolite-supported CdS–PbS photocatalyst [125].

ZnS–NiS-supported clinoptilolite exhibits higher photocatalytic activity concerning non-hybridized ZnS and NiS semiconductors in the degradation of 2-nitrotoluene. The weight ratio of ZnS/NiS significantly affects the photocatalytic activity of the prepared catalyst. The catalyst with 9.7 wt.% ZnS and 3.0 wt.% NiS was the most active. Also, supporting the hybridized system onto clinoptilolite nanoparticles significantly increases its photocatalytic activity compared to unsupported ones. This confirms the ability of the zeolite support to prevent the recombination of the produced electron–hole pairs by migration of the conductance band electrons to the zeolite structure [126].

3. Conclusions

The review demonstrates that natural clinoptilolite is a suitable substrate for immobilizing semiconductor particles with photocatalytic activity. Various techniques can be employed to achieve immobilization. Most procedures rely on ion exchange, where the ions of alkali and alkaline earth metals in the clinoptilolite lattice are substituted with cations found in the semiconductor. During the second step of the procedure, the lattice porosity and accurately determined cation positions facilitate the creation of nano-sized oxides, sulfides, or halides that are evenly distributed. There are several reasons why this contributes to the increase in photocatalytic activity of the semiconductor particles. Firstly, the specific surface area of the semiconductor increases. Secondly, the recombination of electrons and holes slows down. Lastly, the recovery of the catalyst becomes easier.

Various photocatalytic composites have been created, and their effectiveness in breaking down different organic pollutants, primarily in wastewater, has been evaluated. However, further research is necessary in this field as zeolite-based photocatalysts are currently in the early stages of investigation. To further improve the adsorption capacity and photocatalytic activity, suitable semiconductors must be developed, and additional research on the role of zeolite must be conducted. It is also crucial to develop reliable zeolite-based photocatalysts that exhibit high performance when exposed to visible or sunlight irradiation and are used in natural environments.

Author Contributions: Conceptualization, N.R.; methodology, N.R. and J.P.; writing, N.R. and J.P.; writing—review and editing: N.R. and J.P.; Visualization, J.P.; supervision, N.R. All authors have read and agreed to the published version of the manuscript.

Funding: This research was funded by the Ministry of Science, Technological Development and Innovation of the Republic of Serbia (Project number: 451-03-66/2024-03/200011).

Data Availability Statement: The data is contained within the article.

Acknowledgments: The authors express their sincere gratitude to Nenad Blagojević for his technical assistance refining the manuscript.

Conflicts of Interest: The authors declare no conflicts of interest.

References

1. Mamulová Kutláková, K.; Tokarský, J.; Kovář, P.; Vojtěšková, S.; Kovářová, A.; Smetana, B.; Kukutschová, J.; Čapková, P.; Matějka, V. Preparation and characterization of photoactive composite kaolinite/TiO_2. *J. Hazard. Mater.* **2011**, *188*, 212–220. https://doi.org/10.1016/j.jhazmat.2011.01.106.
2. Castañeda-Contreras, J.; Marañón-Ruiz, V.F.; Chiu-Zárate, R.; Pérez-Ladrón de Guevara, H.; Rodriguez, R.; Michel-Uribe, C. Photocatalytic activity of erbium-doped TiO_2 nanoparticles immobilized in macro-porous silica films. *Mater. Res. Bull.* **2012**, *47*, 290–295. https://doi.org/10.1016/j.materresbull.2011.11.021.
3. Wang, C.; Shi, H.; Li, Y. Synthesis and characterization of natural zeolite supported Cr-doped TiO_2 photocatalysts. *Appl. Surf. Sci.* **2012**, *258*, 4328–4333. https://doi.org/10.1016/j.apsusc.2011.12.108.
4. Guimarães, V.; Teixeira, A.R.; Lucas, M.S.; Silva, A.M.T.; Peres, J.A. Pillared interlayered natural clays as heterogeneous photocatalysts for H_2O_2-assisted treatment of a winery wastewater. *Sep. Purif. Technol.* **2019**, *228*, 115768. https://doi.org/10.1016/j.seppur.2019.115768.
5. Mekatel, E.; Trari, M.; Nibou, D.; Sebai, I.; Amorkrane, S. Preparation and characterization of α-Fe_2O_3 supported clay as a novel photocatalyst for hydrogen evolution. *Int. J. Hydrogen Energy* **2019**, *44*, 10309–10315. https://doi.org/10.1016/j.ijhydene.2019.03.007.
6. Alakhras, F.; Alhajri, E.; Haounati, R.; Ouachtak, H.; Ait Addi, A.; Saleh, T.A. A comparative study of photocatalytic degradation of Rhodamine B using natural-based zeolite composites. *Surf. Interfaces* **2020**, *20*, 100611. https://doi.org/10.1016/j.surfin.2020.100611.
7. Hass Caetano Lacerda, E.; Casanova Monteiro, F.; Regina Kloss, J.; Fujiwara, S.T. Bentonite clay modified with Nb_2O_5: An efficient and reused photocatalyst for the degradation of reactive textile dye. *J. Photochem. Photobiol. A Chem.* **2020**, *388*, 112084. https://doi.org/10.1016/j.jphotochem.2019.112084.
8. Khennaouia, B.; Zehani, F.; Malouki, M.; Menacerd, R.; Canle, M. Chemical and physical characterization of a natural clay and its use as photocatalyst for the degradation of the methabenzthiazuron herbicide in water. *Optik* **2020**, *219*, 165024. https://doi.org/10.1016/j.ijleo.2020.165024.
9. Fatimah, I.; Ardianti, S.; Sahroni, I.; Purwiandono, G.; Sagadevan, S.; Doong, R.A. Visible light sensitized porous clay heterostructure photocatalyst of zinc-silica modified montmorillonite by using tris (2,2′-bipyridyl) dichlororuthenium. *Appl. Clay Sci.* **2021**, *204*, 106023. https://doi.org/10.1016/j.clay.2021.106023.
10. Wang, H.; Li, X.; Zhao, X.; Li, C.; Song, X.; Zhang, P.; Huo, P.; Li, X. A review on heterogeneous photocatalysis for environmental remediation: From semiconductors to modification strategies. *Chin. J. Catal.* **2022**, *43*, 178–214. https://doi.org/10.1016/S1872-2067(21)63910-4.
11. Malato, S.; Fernández-Ibánez, P.; Maldonado, M.I.; Blanco, J.; Gernjak, W. Decontamination and disinfection of water by solar photocatalysis: Recent overview and trends. *Catal. Today* **2009**, *147*, 1–59. https://doi.org/10.1016/j.cattod.2009.06.018.
12. Zhu, S.; Wang, D. Photocatalysis: Basic Principles, Diverse Forms of Implementations and Emerging Scientific Opportunities. *Adv. Energy Mater.* **2017**, *7*, 17100841. https://doi.org/10.1002/aenm.201700841.
13. Yang, X.; Wang, D. Photocatalysis: From fundamental principles to materials and applications. *ACS Appl. Energy Mater.* **2018**, *1*, 6657–6693. https://doi.org/10.1021/acsaem.8b01345.
14. Loeb, S.K.; Alvarez, P.J.J.; Brame, J.A.; Cates, E.L.; Choi, W.; Crittenden, J.; Dionysiou, D.D.; Li, Q.; Li-Puma, G.; Quan, X.; et al. The technology horizon for photocatalytic water treatment: Sunrise or Sunset? *Environ. Sci. Technol.* **2019**, *53*, 2937–2947. https://doi.org/10.1021/acs.est.8b05041.
15. Ren, G.; Han, H.; Wang, Y.; Liu, S.; Zhao, J.; Meng, X.; Li, Z. Recent Advances of Photocatalytic Application in Water Treatment: A Review. *Nanomaterials* **2021**, *11*, 1804. https://doi.org/10.3390/nano11071804.
16. Mohod, A.V.; Imran, M.; Momotzko, M.; Shah, N.S.; Marchel, M.; Imram, M.; Kong, L.; Boczkaj, G. Degradation of Rhodamine dyes by Advanced Oxidation Processes (AOPs)—Focus on cavitation and photocatalysis—A critical review. *Water Resour. Ind.* **2023**, *30*, 100220. https://doi.org/10.1016/j.wri.2023.100220.
17. Miklos, D.B.; Remy, C.; Jekel, M.; Linden, K.G.; Drewes, J.E.; Hübner, U. Evaluation of advanced oxidation processes for water and wastewater treatment—A critical review. *Water Res.* **2018**, *139*, 118–131. https://doi.org/10.1016/j.watres.2018.03.042.
18. Dong, C.; Fang, W.; Yi, Q.; Zhang, J. A comprehensive review on reactive oxygen species (ROS) in advanced oxidation processes (AOPs). *Chemosphere* **2022**, *308*, 136205. https://doi.org/10.1016/j.chemosphere.2022.136205.
19. Hassaan, M.A.; El-Nemr, A.; Elkatory, M.R.; Ragab, S.; Niculescu, V.C.; El Nemr, A. Principles of photocatalysts and their different applications: A Review. *Top Curr. Chem.* **2023**, *381*, 31. https://doi.org/10.1007/s41061-023-00444-7.
20. Mahbub, P.; Duke, M. Scalability of advanced oxidation processes (AOPs) in industrial applications: A review. *J. Environ. Manag.* **2023**, *345*, 118861. https://doi.org/10.1016/j.jenvman.2023.118861.

21. Friedmann, R. A General overview of heterogeneous photocatalysis as a remediation technology for wastewaters containing pharmaceutical compounds. *Water* **2022**, *14*, 3588. https://doi.org/10.3390/w14213588.
22. Huang, D.; Chen, S.; Zeng, G.; Gong, X.; Zhou, C.; Cheng, M.; Xue, W.; Yan, X.; Li, J. Artificial Z-scheme photocatalytic system: What have been done and where to go? *Coordin. Chem. Rev.* **2019**, *385*, 44–80. https://doi.org/10.1016/j.ccr.2018.12.013.
23. Tahir, M.; Tasleem, S.; Tahir, B. Recent development in band engineering of binary semiconductor materials for solar driven photocatalytic hydrogen production. *Int. J. Hydrogen Energy* **2020**, *45*, 15985–16038. https://doi.org/10.1016/j.ijhydene.2020.04.071.
24. Yin, S.; Sun, L.; Zhou, Y.; Li, X.; Li, J.; Song, X.; Huo, P.; Wang, H.; Yan, Y. Enhanced electron–hole separation in SnS_2/Au/g-C_3N_4 embedded structure for efficient CO_2 photoreduction. *Chem. Eng. J.* **2021**, *406*, 126776. https://doi.org/10.1016/j.cej.2020.126776.
25. Brame, J.; Long, M.; Li, Q.; Alvarez, P. Inhibitory effect of natural organic matter or other background constituents on photocatalytic advanced oxidation processes: Mechanistic model development and validation. *Water Res.* **2015**, *84*, 362–371. https://doi.org/10.1016/j.watres.2015.07.044.
26. Rezaei, R.; Mohsemi, M. Impact of natural organic matter on the degradation of 2,4-dichlorophenoxy acetic acid in a fluidized bed photocatalytic reactor. *Chem. Eng. J.* **2017**, *310*, 457–463. https://doi.org/10.1016/j.cej.2016.05.086.
27. Lado Ribeira, A.R.; Moreiraa, N.F.F.; Li Puma, G.; Silva, A.M.T. Impact of water matrix on the removal of micropollutants by advanced oxidation technologies. *Chem. Eng. J.* **2019**, *363*, 155–173. https://doi.org/10.1016/j.cej.2019.01.080.
28. Corma, A.; Garcia, H. Zeolite-based photocatalysts. *Chem. Commun.* **2004**, *13*, 1443–1459. https://doi.org/10.1039./B400147H.
29. Sandoval-Díaz, L.-E.; González-Amaya, J.-A.; Carlos-Alexander Trujillo, C.-A. General aspects of zeolite acidity characterization. *Micropor. Mesopor. Mater.* **2015**, *215*, 229–243. https://doi.org/10.1016/j.micromeso.2015.04.038.
30. Reeve, P.J.; Fallowfield, H.J. Natural and surfactant modified zeolites: A review of their applications for water remediation with a focus on surfactant desorption and toxicity towards microorganisms. *J. Environ. Manag.* **2018**, *205*, 253–261. https://doi.org/10.1016/j.jenvman.2017.09.077.
31. Hu, G.; Yang, J.; Duan, X.; Farnood, R.; Yang, C.; Yang, J.; Liu, W.; Liu, Q. Recent developments and challenges in zeolite-based composite photocatalysts for environmental applications. *Chem. Eng. J.* **2021**, *417*, 129209. https://doi.org/10.1016/j.cej.2021.129209.
32. Liaquat, I.; Munir, R.; Fazila Younas, F.; Abbasi, N.A.; Sadia, B.; Muneer, A.; Younas, F.; Sardar, M.F.; Zahid, M.; Noreen, S. Exploring zeolite-based composites in adsorption and photocatalysis for toxic wastewater treatment: Preparation, mechanisms, and future perspectives. *Environ. Pollut.* **2024**, *349*, 123922. https://doi.org/10.1016/j.envpol.2024.123922.
33. Godelitsas, A.; Armbruster, T. HEU-type zeolites modified by transition elements and lead. *Micropor. Mesopor. Mater.* **2003**, *61*, 3–24. https://doi.org/10.1016/S1387-1811(03)00352-4.
34. Dziedzicka, A.; Sulikowski, B.; Ruggiero-Mikolajczyk, M. Catalytic and physicochemical properties of modified natural clinoptilolite. *Catal. Today* **2016**, *259*, 50–58. https://doi.org/10.1016/j.cattod.2015.04.039.
35. Johnson, M.; O'Connor, D.; Barnes, P.; Bell, R.; Catlow, C.R.A.; Owens, S.L.; Sankar, G.; Teat, S.J.; Stephenson, R. Cation exchange, dehydration and calcination in clinoptilolite: In situ X-ray diffraction and computer modeling. *J. Phys. Chem. B* **2003**, *107*, 942–951. https://doi.org/10.1021/jp021672.
36. Snellings, R.A.; Gualtieri, A.F.; Elsen, J. The Rietveld structure refinement of an exceptionally pure sample of clinoptilolite from Ecuador and its Na-, K-, and Ca-exchanged forms. In Eleventh European Powder Diffraction Conference. *Z. Kristallogr. Suppl.* **2009**, *30*, 395–400. https://doi.org/10.1524/zksu.2009.0058.
37. Farías, T.; Ruiz-Salvador, A.R.; Velazco, L.; de Ménorval, L.C.; Rivera, A. Preparation of natural zeolitic supports for potential biomedical applications. *Mater. Chem. Phys.* **2009**, *118*, 322–328. https://doi.org/10.1016/j.matchemphys.2009.07.054.
38. Garcia-Basabe, Y.; Rodriguez-Iznaga, I.; de Menorval, L.-C.; Llewellyn, P.; Maurin, G.; Lewis, D.W.; Binions, R.; Autie, M.; Ruiz-Salvador, A.R. Step-wise dealumination of natural clinoptilolite: Structural and physicochemical characterization. *Micropor. Mesopor. Mater.* **2010**, *135*, 187–196. https://doi.org/10.1016/j.micromeso.2010.07.008.
39. Pavlovic, J.; Popova, M.; Mihalyi, R.M.; Mazaj, M.; Mali, G.; Kovač, J.; Lazarova, H.; Rajic, N. Catalytic activity of SnO_2- and SO_4/SnO_2-containing clinoptilolite in the esterification of levulinic acid. *Micropor. Mesopor. Mater.* **2019**, *279*, 10–18. https://doi.org/10.1016/j.micromeso.2018.12.009.
40. Lin, H.; Liu, Q.; Dong, Y.; He, Y.; Wang, L. Physicochemical properties and mechanism study of clinoptilolite modified by NaOH, *Micropor. Mesopor. Mater.* **2015**, *218*, 174–179. https://doi.org/10.1016/j.micromeso.2015.07.017.
41. De Souza, V.C.; Villarroel-Rocha, J.; De Araújo, M.J.G.; Sapag, K.; Pergher, S.B.C. Basic treatment in natural clinoptilolite for improvement of physicochemical properties. *Minerals* **2018**, *8*, 595. https://doi.org/10.3390/min8120595.
42. Ates, A. Effect of alkali-treatment on the characteristics of natural zeolites with different compositions. *J. Colloid Interf. Sci.* **2018**, *523*, 266–281. https://doi.org/10.1016/j.jcis.2018.03.115.
43. Wang, C.; Leng, S.; Guo, H.; Cao, L.; Huang, J. Acid and alkaline treatments for regulation of hydrophilicity/hydrophobicity of natural zeolite. *Appl. Surf. Sci.* **2019**, *478*, 319–326. https://doi.org/10.1016/j.apsusc.2019.01.263.
44. Pavlović, J.; Hrenović, J.; Povrenović, D.; Rajić, N. Advances in the applications of clinoptilolite-rich tuffs. *Materials* **2024**, *17*, 1306. https://doi.org/10.3390/ma17061306.
45. Rajic, N.; Stojakovic, D.; Daneu, N.; Recnik, A. The formation of oxide nanoparticles on the surface of natural clinoptilolite. *J. Phys. Chem. Solids* **2011**, *72*, 800–803. https://doi.org/10.1016/j.jpcs.2011.03.018.

46. Nezamzadeh-Ejhieh, A.; Moazzeni, N. Sunlight photodecolorization of a mixture of Methyl Orange and Bromocresol Green by CuS incorporated in a clinoptilolite zeolite as a heterogeneous catalyst. *J. Ind. Eng. Chem.* **2013**, *19*, 1433–1442. https://doi.org/10.1016/j.jiec.2013.01.006.
47. Jafari, S.; Nezamzadeh-Ejhieh, A. Supporting of coupled silver halides onto clinoptilolite nanoparticles as simple method for increasing their photocatalytic activity in heterogeneous photodegradation of mixture of 4-methoxy aniline and 4-chloro-3-nitro aniline. *J. Colloid Interface Sci.* **2017**, *490*, 478–487. https://doi.org/10.1016/j.jcis.2016.11.087.
48. Gharbalifard, M.; Nezamzadeh-Ejhieh, A. Synergistic photocatalytic activity of PbS/clinoptilolite in ciprofloxacin photodegradation: An experimental design study. *J. Photochem. Photobiol. A* **2024**, *446*, 115159. https://doi.org/10.1016/j.jphotochem.2023.115159.
49. Heidari, Z.; Alizadeh, R.; Ebadi, A.; Oturan, N.; Oturan, M.A. Efficient photocatalytic degradation of furosemide by a novel sonoprecipited ZnO over ion exchanged clinoptilolite nanorods. *Sep. Purif. Technol.* **2020**, *242*, 116800. https://doi.org/10.1016/j.seppur.2020.116800.
50. Shen, Y.; Zhou, P.; Zhao, S.; Li, A.; Chen, Y.; Bai, J.; Han, C.; Wei, D.; Ao, Y. Synthesis of high-efficient TiO_2/clinoptilolite photocatalyst for complete degradation of xanthate. *Miner. Eng.* **2020**, *159*, 106640. https://doi.org/10.1016/j.mineng.2020.106640.
51. Ullah, R.; Liu, C.; Panezai, H.; Gul, A.; Sun, J.; Wu, X. Controlled crystal phase and particle size of loaded-TiO_2 using clinoptiloliteas support via hydrothermal method for degradation of crystal violet dye in aqueous solution. *Arab. J. Chem.* **2020**, *13*, 4092–4101. https://doi.org/10.1016/j.arabjc.2019.06.011.
52. Ullah, R.; Sun, J.; Gul, A.; Munir, T.; Wu, X. Evaluations of physico-chemical properties of TiO_2/clinoptilolite synthesized via three methods on photocatalytic degradation of crystal violet. *Chin. J. Chem. Eng.* **2021**, *33*, 181–189. https://doi.org/10.1016/j.cjche.2020.09.045.
53. Karunakaran, C.; Senthilvelan, S.; Karuthapandian, S. TiO_2—Photocatalyzed oxidation of aniline. *J. Photochem. Photobiol. A* **2005**, *172*, 207–213. https://doi.org/10.1016/j.jphotochem.2004.12.010.
54. Chen, K.; Li, J.; Li, J.; Zhang, Y.; Wang, W. Synthesis and characterization of TiO_2–montmorillonites doped with vanadium and/or carbon and their application for the photodegradation of sulphorhodamine B under UV–vis irradiation. *Colloid Surf. A* **2010**, *360*, 47–56. https://doi.org/10.1016/j.colsurfa.2010.02.005.
55. Kang, X.; Liu, S.; Dai, Z.; He, Y.; Song, X.; Tan, Z. Titanium Dioxide: From Engineering to Applications. *Catalysts* **2019**, *9*, 191. https://doi.org/10.3390/catal9020191.
56. Liang, Y.; Huang, G.; Xin, X.; Yao, Y.; Li, Y.; Yin, J.; Li, X.; Wu, Y.; Gao, S. Black titanium dioxide nanomaterials for photocatalytic removal of pollutants: A review. *J. Mater. Sci. Technol.* **2022**, *112*, 239–262. https://doi.org/10.1016/j.jmst.2021.09.057.
57. Akbari Sene, R.; Sharifnia, S.; Moradi, G.R. On the impact evaluation of various chemical treatments of support on the photocatalytic properties and hydrogen evolution of sonochemically synthesized TiO_2/Clinoptilolite. *Int. J. Hydrogen Energy* **2018**, *43*, 695–707. https://doi.org/10.1016/j.ijhydene.2017.11.099.
58. Elghniji, K.; Elaloui, E.; Moussaoui, Y. Coating of anatase titania on clinoptilolite by metal organic chemical vapor deposition method: Enhanced mesoporosity and photocatalytic activity. *Chem. Pap.* **2018**, *72*, 1159–1168. https://doi.org/10.1007/s11696-017-0350-1.
59. Castañeda-Juárez, M.; Martínez-Miranda, V.; Almazán-Sánchez, P.T.; Linares-Hernández, I.; Santoyo-Tepole, F.; Vázquez-Mejía, G. Synthesis of TiO_2 catalysts doped with Cu, Fe, and Fe/Cu supported on clinoptilolite zeolite by an electrochemical-thermal method for the degradation of diclofenac by heterogeneous photocatalysis. *J. Photochem. Photobiol. A Chem.* **2019**, *380*, 111834. https://doi.org/10.1016/j.jphotochem.2019.04.045.
60. Zabihi-Mobarakeh, H.; Nezamzadeh-Ejhieh, A. Application of supported TiO_2 onto Iranian clinoptilolite nanoparticles in the photodegradation of mixture of aniline and 2,4-dinitroaniline aqueous solution. *J. Ind. Eng. Chem.* **2015**, *26*, 315–321. https://doi.org/10.1016/j.jiec.2014.12.003.
61. Ko, S.; Fleming, P.D.; Joyce, M.; Ari-Gur, P. High performance nano-titania photocatalytic paper composite. Part II: Preparation and characterization of natural zeolite-based nano-titania composite sheets and study of their photocatalytic activity. *Mater. Sci. Eng. B-Adv.* **2009**, *164*, 135–139. https://doi.org/10.1016/j.mseb.2009.08.010.
62. Khodadoust, S.; Sheini, A.; Armand, N. Photocatalytic degradation of monoethanolamine in wastewater using nanosized TiO_2 loaded on clinoptilolite. *Spectrochim. Acta Part A* **2012**, *92*, 91–95. https://doi.org/10.1016/j.saa.2012.01.082.
63. Liu, X.; Liu, Y.; Lu, S.; Guo, W.; Xi, B. Performance and mechanism into TiO_2/Zeolite composites for sulfadiazine adsorption and photodegradation. *Chem. Eng. J.* **2018**, *350*, 131–147. https://doi.org/10.1016/j.cej.2018.05.141.
64. Sanni, S.O.; Modise, S.J.; Viljoen, E.L.; Ofomaja, A.E. Enhanced degradation of dye mixtures: Physicochemical and electrochemical properties of titania dispersed on clinoptilolite, synergistic influence. *SN Appl. Sci.* **2020**, *2*, 1668. https://doi.org/10.1007/s42452-020-03398-3.
65. Yener, H.B.; Yılmaz, M.; Deliismail, Ö.; Özkan, S.F.; Helvacı, Ş.Ş. Clinoptilolite supported rutile TiO_2 composites: Synthesis, characterization, and photocatalytic activity on the degradation of terephthalic acid. *Sep. Purif. Technol.* **2017**, *173*, 17–26. https://doi.org/10.1016/j.seppur.2016.09.010.
66. Tan, Y.; Li, C.; Sun, Z.; Liang, C.; Zheng, S. Ternary structural assembly of BiOCl/TiO_2/clinoptilolite composite: Study of coupled mechanism and photocatalytic performance. *J. Colloid Interface Sci.* **2020**, *564*, 143–154. https://doi.org/10.1016/j.jcis.2019.12.116.
67. Zhou, P.; Shen, Y.; Zhao, S.; Chen, Y.; Gao, S.; Liu, W.; Wei, D. Hydrothermal synthesis of novel ternary hierarchical MoS_2/TiO_2/clinoptilolite nanocomposites with remarkably enhanced visible light response towards xanthates. *Appl. Surf. Sci.* **2021**, *542*, 148578. https://doi.org/10.1016/j.apsusc.2020.148578.

68. Zhou, P.; Shen, Y.; Zhao, S.; Bai, J.; Han, C.; Liu, W.; Wei, D. Facile synthesis of clinoptilolite-supported Ag/TiO_2 nanocomposites for visible-light degradation of xanthates. *J. Taiwan Inst. Chem. Eng.* **2021**, *122*, 231–240. https://doi.org/10.1016/j.jtice.2021.04.049.
69. Amiri, S.; Anbia, M. Insights into the effect of parameters and pathway of visible-light photodegradation of glyphosate and diazinon by C-TiO_2/clinoptilolite nanocomposite. *J. Photochem. Photobiol. A* **2024**, *446*, 115146. https://doi.org/10.1016/j.jphotochem.2023.115146.
70. Ali Johar, M.; Arslan Afzal, R.; Ali Alazba, A.; Manzoor, U. Photocatalysis and bandgap engineering using ZnO nanocomposites. *Adv. Mater. Sci. Eng.* **2015**, *2015*, 934587. https://doi.org/10.1155/2015/934587.
71. Chen, X.; Wu, Z.; Liu, D.; Gao, Z. Preparation of ZnO Photocatalyst for the efficient and rapid photocatalytic degradation of azo dyes. *Nanoscale Res. Lett.* **2017**, *12*, 143. https://doi.org/10.1186/s11671-017-1904-4.
72. Razavi-Khosroshahi, H.; Edalati, K.; Wu, J.; Nakashima, Y.; Arita, M.; Ikoma, Y.; Sadakiyo, M.; Inagaki, Y.; Staykov, A.; Yamauchi, Y.; et al. High-pressure zinc oxide phase as visible-light-active photocatalyst with narrow band gap. *J. Mater. Chem. A* **2017**, *5*, 20298–20303. https://doi.org/10.1039/c7ta05262f.
73. Lee, S.J.; Jung, H.J.; Koutavarapu, R.; Lee, S.H.; Arumugam, M.; Kim, J.H.; Choi, M.Y. ZnO supported Au/Pd bimetallic nanocomposites for plasmon improved photocatalytic activity for methylene blue degradation under visible light irradiation. *Appl. Surf. Sci.* **2019**, *496*, 143665. https://doi.org/10.1016/j. apsusc.2019.143665.
74. Taha, A.; Da'na, E.; Hassanin, H.A. Modified activated carbon loaded with bio-synthesized Ag/ZnO nanocomposite and its application for the removal of Cr (VI) ions from aqueous solution. *Surf. Interfaces* **2021**, *23*, 100928. https://doi.org/10.1016/j.surfin.2021.100928.
75. Jagannatha, R.B.; Rani, R.S.; Padaki, M. ZnO zeolite nanocomposite for photocatalytic elimination of benzophenone and caffeine. *ChemistrySelect* **2019**, *4*, 1989–1993. https://doi.org/10.1002/slct.201804006.
76. Nezamzadeh-Ejhieh, A.; Khorsandi, S. Photocatalytic degradation of 4-nitrophenol with ZnO supported nano-clinoptilolite zeolite. *J. Ind. Eng. Chem.* **2014**, *20*, 937–946. https://doi.org/10.1016/j.jiec.2013.06.026.
77. Iazdani, F.; Nezamzadeh-Ejhieh, A. The photocatalytic rate of ZnO supported onto natural zeolite nanoparticles in the photodegradation of an aromatic amine. *Environ. Sci. Pollut. Res.* **2021**, *28*, 53314–53327. https://doi.org/10.1007/s11356-021-14544-8.
78. Nezamzadeh-Ejhieh, A.; Khodabakhshi-Chermahini, F. Incorporated ZnO onto nano clinoptilolite particles as the active centers in the photodegradation of phenylhydrazine. *J. Ind. Eng. Chem.* **2014**, *20*, 695–704. https://doi.org/10.1016/j.jiec.2013.05.035.
79. Bahrami, M.; Nezamzadeh-Ejhieh, A. Effect of the supported ZnO on clinoptilolite nano-particles in the photodecolorization of semi-real sample bromothymol blue aqueous solution. *Mater. Sci. Semicond. Process.* **2015**, *30*, 275–284. https://doi.org/10.1016/j.mssp.2014.10.006.
80. De Dios, F.S.; Morales, E.R.; Cortaza, M.D.A.; Hernández, G.P.; Mandujano, E.V.M.; Alejandro, E.M.L.; Blanco, L.R. Improvement of photocatalysis using ZnO/zeolite nanocomposites for contaminant removal in aqueous media. *Desalin. Water Treat.* **2023**, *312*, 79–88. https://doi.org/10.5004/dwt.2023.29961.
81. Da Silvaa, P.L.; Nippes, R.P.; Macruz, P.D.; Hegetob, F.L.; Scaliante, M.H.N.O. Photocatalytic degradation of hydroxychloroquine using ZnO supported on clinoptilolite zeolite. *Water Sci. Technol.* **2021**, *84*, 764. https://doi.org/10.2166/wst.2021.265.
82. Wahyuni, T.H.; Diantariani, N.P.; Kartini, I.; Kuncaka, A. Enhancement of the photostability and visible photoactivity of ZnO photocatalyst used for reduction of Cr(VI) ions. *Results Eng.* **2022**, *13*, 100351. https://doi.org/10.1016/j.rineng.2022.100351.
83. Bahrami, M.; Nezamzadeh-Ejhieh, A. Effect of supporting and hybridizing of FeO and ZnO semiconductors onto an Iranian clinoptilolite nano-particles and the effect of ZnO/FeO ratio in the solar photodegradation of fish ponds waste water. *Mat. Sci. Semicon. Proc.* **2014**, *27*, 833–840. https://doi.org/10.1016/j.mssp.2014.08.030.
84. Verma, N.; Kumar, N. Synthesis and Biomedical Applications of Copper Oxide Nanoparticles: An Expanding Horizon. *ACS Biomater. Sci. Eng.* **2019**, *5*, 1170–1188. https://doi.org/10.1021/acsbiomaterials.8b01092.
85. Katal, R.; Masudy-Panah, S.; Kong, E.Y.-J.; Khiavi, N.D.; DavoodAbadi Farahani, M.H.; Gong, X. Nanocrystal-engineered thin CuO film photocatalyst for visible-light-driven photocatalytic degradation of organic pollutant in aqueous solution. *Catal. Today* **2020**, *40*, 236–244. https://doi.org/10.1016/j.cattod.2018.12.019.
86. Soori, F.; Nezamzadeh-Ejhieh, A. Synergistic effects of copper oxide-zeolite nanoparticles composite on photocatalytic degradation of 2,6-dimethylphenol aqueous solution. *J. Mol. Liq.* **2018**, *255*, 250–256. https://doi.org/10.1016/j.molliq.2018.01.169.
87. Saberian, M.; Nezamzadeh-Ejhieh, A. Synergistic photocatalytic degraded tetracycline upon supported CuO clinoptilolite nanoparticles. *Solid State Sci.* **2024**, *147*, 107381. https://doi.org/10.1016/j.solidstatesciences.2023.107381.
88. Nezamzadeh-Ejhieh, A.; Zabihi-Mobarakeh, H. Heterogeneous photodecolorization of mixture of methylene blue and bromophenol blue using CuO-nano-clinoptilolite. *J. Ind. Eng. Chem.* **2014**, *20*, 1421–1431. https://doi.org/10.1016/j.jiec.2013.07.027.
89. Iazdani, F.; Nezamzadeh-Ejhieh, A. Supported cuprous oxide-clinoptilolite nanoparticles: Brief identification and the catalytic kinetics in the photodegradation of dichloroaniline. *Spectrochim. Acta Part A Mol. Biomol. Spectrosc.* **2021**, *250*, 119348. https://doi.org/10.1016/j.saa.2020.119348.
90. Nezamzadeh-Ejhieh, A.; Amiri, M. CuO supported Clinoptilolite towards solar photocatalytic degradation of p-aminophenol. *Powder Technol.* **2013**, *235*, 279–288. https://doi.org/10.1016/j.powtec.2012.10.017.
91. Amiri, M.; Nezamzadeh-Ejhieh, A. Improvement of the photocatalytic activity of cupric oxide by deposition onto a natural clinoptilolite substrate. *Mat.Sci. Semicon. Proc.* **2015**, *31*, 501–508. https://doi.org/10.1016/j.mssp.2014.12.030.

92. Shirzadi, A.; Nezamzadeh-Ejhieh, A. Enhanced photocatalytic activity of supported CuO–ZnO semiconductors towards the photodegradation of mefenamic acid aqueous solution as a semi real sample. *J. Mol. Catal. A-Chem.* **2016**, *411*, 222–229. https://doi.org/10.1016/j.molcata.2015.10.027.
93. Dashtpeyma, G.; Shabanian, S.R. Efficient photocatalytic oxidative desulfurization of liquid petroleum fuels under visible-light irradiation using a novel ternary heterogeneous $BiVO_4$-CuO/modified natural clinoptilolite zeolite. *J. Photochem. Photobiol. A* **2023**, *445*, 115024. https://doi.org/10.1016/j.jphotochem.2023.115024.
94. Zhang, M.; An, T.; Hu, X.; Wang, C.; Sheng, G.; Fu, J. Preparation and photocatalytic properties of a nanometer ZnO–SnO_2 coupled oxide. *Appl. Catal. A-Gen* **2004**, *260*, 215–222. https://doi.org/10.1016/j.apcata.2003.10.025.
95. Kim, S.P.; Choi, M.Y.; Choi, H.C. Photocatalytic activity of SnO_2 nanoparticles in methylene blue degradation. *Mater. Res. Bull.* **2016**, *74*, 85–89. https://doi.org/10.1016/j.materresbull.2015.10.024.
96. Šuligoj, A.; Pavlović, J.; Arčon, I.; Rajić, N.; Novak Tušar, N. SnO_2-containing clinoptilolite as a composite photocatalyst for dyes removal from wastewater under solar light. *Catalysts* **2020**, *10*, 253. https://doi.org/10.3390/catal10020253.
97. Khodami, Z.; Nezamzadeh-Ejhieh, A. Investigation of photocatalytic e_ect of ZnO–SnO_2/nano clinoptilolite system in the photodegradation of aqueous mixture of 4-methylbenzoic acid/2-chloro-5-nitrobenzoic acid. *J. Mol. Catal. A Chem.* **2015**, *409*, 59–68. https://doi.org/10.1016/j.molcata.2015.08.013.
98. Derikvandi, H.; Nezamzadeh-Ejhieh, A. A comprehensive study on electrochemical and photocatalytic activity of SnO_2-ZnO/clinoptilolite nanoparticles. *J. Mol. Catal. A Chem.* **2017**, *426*, 158–169. https://doi.org/10.1016/j.molcata.2016.11.011.
99. Derikvandi, H.; Nezamzadeh-Ejhieh, A. Synergistic effect of p-n heterojunction, supporting and zeolite nanoparticles in enhanced photocatalytic activity of NiO and SnO_2. *J. Colloid Interf. Sci.* **2017**, *490*, 314–327. https://doi.org/10.1016/j.jcis.2016.11.069.
100. Khoshdel, K.; Honarmand, M.; Hassani, H. SnO_2 and CuO anchored on zeolite as an efficient heterojunction photocatalyst for sunlight-assisted degradation of cefixime. *Environ. Sci. Pollut. Res.* **2023**, *30*, 36883–36903. https://doi.org/10.1007/s11356-022-24635-9.
101. Sabouri, Z.; Fereydouni, N.; Akbari, A.; Hosseini, H.A.; Hashemzadeh, A.; Amiri, M.S.; Darroudi, M.; Kazemi Oskuee, R. Plant-based synthesis of NiO nanoparticles using salvia macrosiphon Boiss extract and examination of their water treatment. *Rare Met.* **2020**, *39*, 1134–1144. https://doi.org/10.1007/s12598-019-01333-z.
102. Aejitha, S.; Dhanraj, G.; Govindaraj, T.; Senthil Kumar, N.; Maiz, F.; Shkir, M.; Kim, W.K.; Reddy Minnam Reddy, V.; Kim, D.H. Effect of La-doping on NiO photocatalyst for enhancing photocatalytic degradation performance under visible light irradiation: DFT calculations and degradation mechanism. *Inorg. Chem. Commun.* **2023**, *156*, 111172. https://doi.org/10.1016/j.inoche.2023.111172.
103. Makhado, K.P.; Mphahlele-Makgwane, M.M.; Kumar, N.; Baker, P.G.; Makgwane, P.R. Current updates on p-type nickel oxide (NiO) based photocatalysts towards decontamination of organic pollutants from wastewater. *Mater. Today Sustain.* **2024**, *25*, 100664. https://doi.org/10.1016/j.mtsust.2023.100664.
104. Ajoudanian, N.; Nezamzadeh-Ejhieh, A. Enhanced photocatalytic activity of nickel oxide supported on clinoptilolite nanoparticles for the photodegradation of aqueous cephalexin. *Mater. Sci. Semicond. Process.* **2015**, *36*, 162–169. https://doi.org/10.1016/j.mssp.2015.03.042.
105. Pourtaheri, A.; Nezamzadeh-Ejhieh, A. Enhancement in photocatalytic activity of NiO by supporting onto an Iranian clinoptilolite nano-particles of aqueous solution of cefuroxime pharmaceutical capsule. *Spectrochim. Acta Part A* **2015**, *137*, 338–344. https://doi.org/10.1016/j.saa.2014.08.058.
106. Pourtaheri, A.; Nezamzadeh-Ejhieh, A. Photocatalytic properties of incorporated NiO onto clinoptilolite nano-particles in the photodegradation process of aqueous solution of cefixime pharmaceutical capsule. *Chem. Eng. Res. Des.* **2015**, *104*, 835–843. https://doi.org/10.1016/j.cherd.2015.10.031.
107. Arabpour, N.; Nezamzadeh-Ejhieh, A. Photodegradation of cotrimaxazole by clinoptilolite-supported nickel oxide. *Process Saf. Environ. Prot.* **2016**, *102*, 431–440. https://doi.org/10.1016/j.psep.2016.04.025.
108. Iazdani, F.; Nezamzadeh-Ejhieh, A. Photocatalytic kinetics of 2,4-dichloroaniline degradation by NiO-clinoptilolite nanoparticles. *Spectrochim. Acta A* **2021**, *250*, 119228. https://doi.org/10.1016/j.saa.2020.119228.
109. Liu, J.; Xue, D. Solvothermal synthesis of CuS semiconductor hollow spheres based on a bubble template route. *J. Cryst. Growth* **2009**, *311*, 500–503. https://doi.org/10.1016/j.jcrysgro.2008.09.025.
110. Mageshwari, K.; Mali, S.S.; Hemalatha, T.; Sathyamoorthy, R.; Patil, P.S. Low temperature growth of CuS nanoparticles by reflux condensation method. *Prog. Solid State Chem.* **2011**, *39*, 108–113. https://doi.org/10.1016/j.progsolidstchem.2011.10.003.
111. Isik, M.; Terlemezoglu, M.; Gasanly, N.; Parlak, M. Structural, morphological and temperature-tuned bandgap characteristics of CuS nano-flake thin films. *Phys. E* **2022**, *144*, 115407. https://doi.org/10.1016/j.physe.2022.115407.
112. Surendran, S.; Vijaya Sankar, K.; Berchmans, J.L.; Kalai Selvan, R. Polyol synthesis of α-NiS particles and its physico-chemical properties. *Mat. Sci. Semicon. Proc.* **2015**, *33*, 16–23. https://doi.org/10.1016/j.mssp.2015.01.012.
113. Fazli, Y.; Pourmortazavi, S.M.; Kohsari, I.; Karimi, M.S.; Tajdari, M. Synthesis, characterization and photocatalytic property of nickel sulfide nanoparticles. *J. Mater. Sci. Mater. Electron.* **2016**, *27*, 7192–7199. http://dx.doi.org/10.1007/s10854-016-4683-2.
114. Hafdi, H.; Mouldar, J.; Joudi, M.; Hatimi, B.; Nasrellah, H.; Mhammedi, M.A.E.; Bakasse, M. Nickel sulfide impregnated on natural phosphate: Characterization and applications in photocatalytic degradation of indigocarmine dye. *Opt. Quant. Electron.* **2021**, *53*, 183. https://doi.org/10.1007/s11082-021-02811-4.

115. Kumar, V.; Sharma, Z.K.; Sharma, K.; Dwivedi, D.K. Investigation on physical properties of polycrystalline nickel sulphide films grown by simple & economical screen-printing method. *Optik* **2018**, *156*, 43–48. https://doi.org/10.1016/j.ijleo.2017.10.169.
116. Muniyappa, M.; Kalegowda, S.N.; Shetty, M.; Sriramoju, I.B.; Shastri, M.; Rao, S.V.N.; De, D.; Shankar, M.V.; Rangappa, D. Cocatalyst free nickel sulphide nanostructure for enhanced photocatalytic hydrogen evolution. *Int. J. Hydrogen Energy* **2022**, *47*, 5307–5318. https://doi.org/10.1016/j.ijhydene.2021.11.171.
117. Nezamzadeh-Ejhieh, A.; Moeinirad, S. Heterogeneous photocatalytic degradation of furfural using NiS-clinoptilolite zeolite. *Desalination* **2011**, *273*, 248–257. https://doi.org/10.1016/j.desal.2010.12.031.
118. Günes, S.; Fritz, K.P.; Neugebauer, H.; Sariciftci, N.S.; Kumar, S.; Scholes, G.D. Hybrid solar cells using PbS nanoparticles. *Sol. Energy Mat. Sol. C* **2007**, *91*, 420–423. https://doi.org/10.1016/j.solmat.2006.10.016.
119. Mamiyev, Z.; Balayeva, N.O. PbS nanostructures: A review of recent advances. *Mater. Today Sustain.* **2023**, *21*, 100305. https://doi.org/10.1016/j.mtsust.2022.100305.
120. Hassan, A.; Zafar, H.K.; Nafady, A.; Sohail, M. Synthesis and characterization of novel ferrocene/PbS nanocomposite material by low-temperature co-precipitation method. *Inorg. Chem. Commun.* **2024**, *162*, 112194. https://doi.org/10.1016/j.inoche.2024.112194.
121. Mehrabanpour, N.; Nezamzadeh-Ejhieh, A.; Ghattavi, S. A comparative photocatalytic activity between PbS NPs and PbS-clinoptilolite towards Cefotaxime. *Solid State Sci.* **2022**, *131*, 106953. https://doi.org/10.1016/j.solidstatesciences.2022.106953.
122. Almanqur, L.; Vitorica-Yrezabal, I.; Whitehead, G.; Lewis, D.; O'Brien, P. Synthesis of nanostructured powders and thin films of iron sulfide from molecular precursors. *RSC Adv.* **2018**, *8*, 29096. https://doi.org/10.1039/c8ra04917c.
123. Rahmani-Aliabadi, A.; Nezamzadeh-Ejhieh, A. A visible light FeS/Fe_2S_3/zeolite photocatalyst towards photodegradation of ciprofloxacin. *J. Photochem. Photobiol. A* **2018**, *357*, 1–10. https://doi.org/10.1016/j.jphotochem.2018.02.006.
124. Azimi, S.; Nezamzadeh-Ejhieh, A. Enhanced activity of clinoptilolite-supported hybridized PbS–CdS semiconductors for the photocatalytic degradation of a mixture of tetracycline and cephalexin aqueous solution. *J. Mol. Catal. A-Chem.* **2015**, *408*, 152–160. https://doi.org/10.1016/j.molcata.2015.07.017.
125. Mehrabanpour, N.; Nezamzadeh-Ejhieh, A.; Ghattavi, S.; Ershadi, A. A magnetically separable clinoptilolite supported CdS-PbS photocatalyst: Characterization and photocatalytic activity toward cefotaxime. *Appl. Surf. Sci.* **2023**, *614*, 156252. https://doi.org/10.1016/j.apsusc.2022.156252.
126. Mohammadyari, P.; Nezamzadeh-Ejhieh, A. Supporting of mixed ZnS–NiS semiconductors onto clinoptilolite nano-particles to improve its activity in photodegradation of 2-nitrotoluene. *RSC Adv.* **2015**, *5*, 75300–75310. https://doi.org/10.1039/C5RA12608H.

.